J. Phys.: Condens. Matter **20** (2008) 304215 (8pp) doi:10.1088/0953-8984/20/30/304215

Plasmonic metamaterials based on holey metallic films

A Mary[1], Sergio G Rodrigo[2], L Martín-Moreno[2] and F J García-Vidal[1]

[1] Departamento de Física de la Materia Condensada, Universidad Autónoma de Madrid, E-28049 Madrid, Spain
[2] Departamento de Física de la Materia Condensada-ICMA, Universidad de Zaragoza-CSIC, E-50009 Zaragoza, Spain

E-mail: fj.garcia@uam.es

Received 11 January 2008
Published 8 July 2008
Online at stacks.iop.org/JPhysCM/20/304215

Abstract

In this paper we address from the fundamental point of view the links and relations between three different phenomena that emerge when metallic films are perforated with periodic arrays of holes: (i) the phenomenon of extraordinary optical transmission in single metallic layers, (ii) the appearance of surface electromagnetic modes (the so-called *spoof* surface plasmons) when an array of holes is drilled on the surface of a perfect electrical conductor and (iii) the negative refractive index behavior observed in double-fishnet (DF) structures in which a periodic hole array is perforated on a metal–dielectric–metal stack. By using a very simple theoretical framework, we show how the physical origin of the negative refractive index in these DF structures is due to the excitation of spoof gap surface plasmon modes that propagate within the dielectric slab. We also demonstrate that the electrical response of the DF system is mainly controlled by the cut-off frequency of the hole waveguide. Finally, we present some results for multilayered DF structures that illustrate how the negative refractive index is maintained when several DF units are stacked together.

(Some figures in this article are in colour only in the electronic version)

1. Introduction

The discovery of the phenomenon of extraordinary optical transmission (EOT) through subwavelength holes by Ebbesen and co-workers [1] has been one of most important findings in the field of optics during the last ten years. It has sparked considerable interest for its fundamental implications and also from the applied point of view, as many potential applications based on this phenomenon have been proposed [2]. The basic structure in which the EOT phenomenon emerges is a two-dimensional (2D) periodic array of subwavelength holes perforated on an optically thick metallic film. This phenomenon is characterized by the appearance of a series of transmission peaks and dips in the transmission spectrum. From the beginning, it was realized that the spectral locations of these resonant features coincide with the corresponding ones of the surface plasmon polaritons (SPPs) [3]. This link between EOT and SPPs has been corroborated by subsequent theoretical works [4, 5] and now it is widely accepted that the excitation of these surface electromagnetic (EM) modes is at the origin of EOT.

The first EOT experiments were performed within the optical regime of the EM spectrum with the period of the array being in the range 400–700 nm. However, it was predicted that the EOT phenomenon could also appear in perforated perfect electrical conductors (PECs) [4]. This hypothesis was experimentally verified by fabricating a 2D hole array in an aluminum sheet with the period of the array being 5 mm [6]. The fact that EOT also emerges in a perforated PEC raised some doubts regarding the origin of EOT, as SPPs cannot be excited on a PEC film. This paradox was resolved in 2004 [7] by demonstrating that, although the surface of a unstructured PEC does not support SPPs, when this surface is drilled with a periodic array of indentations (a periodic array of holes, for example), surface EM modes could exist whose characteristics are very similar to the SPP ones in the optical regime. In fact, it was demonstrated [7] that the dispersion relation of these surface EM modes was governed

by a Drude-like behavior, in which the plasma frequency of the electron gas is replaced by the cut-off frequency of the hole waveguide. This property has important consequences as it opens the possibility of engineering the properties of these surface EM modes by playing with the geometry of the hole array. Due to their mimicking properties with respect to SPPs, these geometry-induced surface EM modes were called *spoof* SPPs.

On the other hand, the seminal paper published almost ten years ago by Pendry and co-workers [8] on the effective negative magnetic susceptibility associated with *metamaterials* formed by arrays of split-ring resonators opened the search for negative refractive index (NRI) materials [9]. In these NRI metamaterials, both the electric permittivity and the magnetic permeability are negative, leading to a refractive index that is negative. Metamaterials presenting NRI are expected to lead to important applications, the perfect lens as proposed also by Pendry [10] being one of the most exciting ones. One of the structures that displays this NRI behavior is the so-called double-fishnet (DF) system, a design very similar to the one showing EOT. The DF structure is composed by a 2D array of holes penetrating completely through a metal–dielectric–metal film stack [11, 12]. Several experiments have shown that this structure presents NRI at visible [13] and near infrared frequencies [14, 15]. Very recent studies have also shown that this negative index metamaterial design also operates in the microwave frequency regime [16, 17].

The aim of this paper is to discover the links and relations between the three phenomena described in the previous three paragraphs (EOT, spoof SPPs and NRI in double-fishnet structures) by analyzing the physical mechanism(s) leading to the NRI response of DF structures. The paper is organized as follows. In section 2, we resume the basic ingredients of the theoretical framework used in this analysis whereas in section 3 we present the main results and findings of our study. The main conclusions of our work are summarized in section 4.

2. Theoretical formalism

In figure 1(a) we render the DF structure analyzed throughout this paper. The DF structure is an infinite square array (period d) of rectangular holes of sides a_x and a_y, perforated on a film composed by two metallic slabs of thickness h_m and a dielectric layer of thickness h_d placed between the two metallic slabs. We are interested in looking at the transmission and reflection properties of this structure under illumination by a p-polarized plane wave. We are also interested in retrieving its effective optical parameters (electric permittivity, ϵ_eff, magnetic permeability, μ_eff, and refractive index, n_eff).

Let us present briefly the basic ingredients of the theoretical framework used to deal with the DF structure. More technical details can be found in [18, 19]. This method is based on a modal expansion of the EM fields in the different regions defining the system. In reflection (I) and transmission (III) vacuum regions the electric fields are expressed in terms of plane waves $|\mathbf{k}\sigma\rangle$, characterized by the in-plane component of the wavevector $\mathbf{k}$ (xy plane) and the polarization σ as

$$|\mathbf{E}_\mathrm{I}(z)\rangle = |\mathbf{k}_0\sigma_0\rangle \mathrm{e}^{\mathrm{i}k_z^0 z} + \sum_{\mathbf{k}\sigma} r_{\mathbf{k}\sigma}|\mathbf{k}\sigma\rangle \mathrm{e}^{\mathrm{i}k_z z} \qquad (1)$$

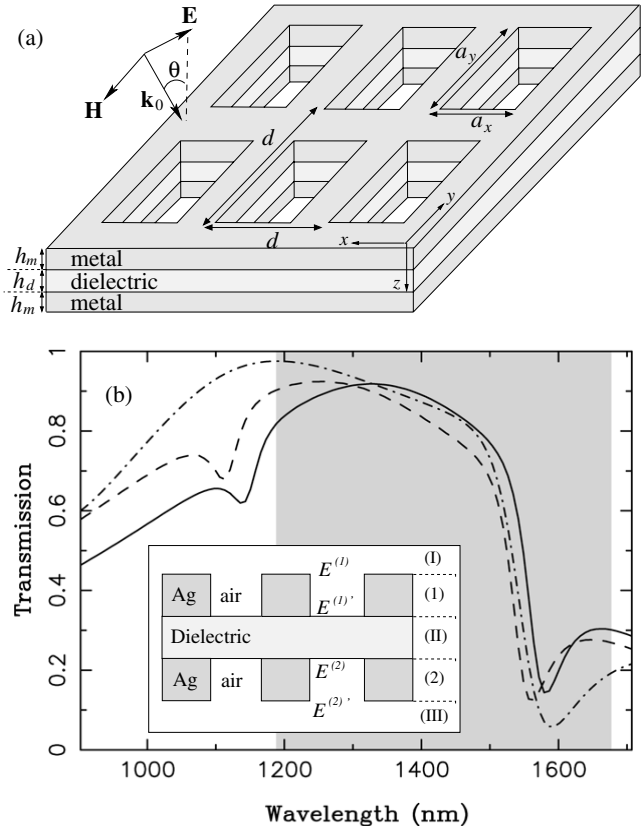

Figure 1. (a) Schematic picture of a DF structure: a square array of rectangular holes of side a_x and a_y perforated on two metallic films of thickness h_m. The perforated films are separated by a dielectric medium of thickness h_d, characterized by a dielectric constant ϵ_d. Parameter d defines the period of the array. The structure with SIBC is illuminated by a p-polarized plane wave. (b) Normal incident transmission spectra for the experimental geometrical parameters of [14] in which the DF structure was made of silver: $a_x = 284$ nm, $a_y = 500$ nm, $d = 600$ nm, $h_\mathrm{m} = 45$ nm, $h_\mathrm{d} = 30$ nm and $\epsilon_\mathrm{d} = 1.9$. FDTD calculations with (dashed line) and without (solid line) holes inside the dielectric layer. Dot–dashed curve: modal expansion calculations. The gray area shows the spectral region where $\mathrm{Re}(n_\mathrm{eff}) < 0$. The inset in this panel shows a schematic representation of the notation used for the modal amplitudes related to the DF structure.

$$|\mathbf{E}_\mathrm{III}(z)\rangle = \sum_{\mathbf{k}\sigma} t_{\mathbf{k}\sigma}|\mathbf{k}\sigma\rangle \mathrm{e}^{\mathrm{i}k_z z} \qquad (2)$$

where $r_\mathbf{k}$ and $t_\mathbf{k}$ define the reflection and transmission coefficients. Region (II) corresponds to the dielectric slab located between the two metallic films. In the experimental samples, this dielectric layer is also perforated by a 2D array of holes. Here, in order to simplify the calculation, we consider this region as a continuous layer. We will show later that similar results are obtained for perforated and non-perforated dielectric layers. Therefore, the electric field can be also expressed in terms of plane waves:

$$|\mathbf{E}_\mathrm{II}(z)\rangle = \sum_{\mathbf{k}\sigma} (\tau_{\mathbf{k}\sigma} + \rho_{\mathbf{k}\sigma})|\mathbf{k}\sigma\rangle \mathrm{e}^{\mathrm{i}k_z z}. \qquad (3)$$

The magnetic fields are related to the electric field through the admittances, $Y_{\mathbf{k},\mathrm{s}} = k_z/k_0$ and $Y_{\mathbf{k},\mathrm{p}} = k_0/k_z$ (for s- and

p-polarization, respectively) where $k_z = \sqrt{k_0^2 - |k|^2}$, k_0 being the wavenumber of the incident plane wave, $k_0 = 2\pi/\lambda$:

$$-\mathbf{u}_z \times |\mathbf{H}_{\mathrm{I}}(z)\rangle = Y_{\mathbf{k}_0,\sigma_0}|\mathbf{k}_0\sigma_0\rangle e^{ik_z^0 z} - \sum_{\mathbf{k}\sigma} r_{\mathbf{k}\sigma} Y_{\mathbf{k},\sigma}|\mathbf{k}\sigma\rangle e^{ik_z z} \quad (4)$$

$$-\mathbf{u}_z \times |\mathbf{H}_{\mathrm{II}}(z)\rangle = \sum_{\mathbf{k}\sigma} (\tau_{\mathbf{k}\sigma} - \rho_{\mathbf{k}\sigma}) Y_{\mathbf{k},\sigma}|\mathbf{k}\sigma\rangle e^{ik_z z} \quad (5)$$

$$-\mathbf{u}_z \times |\mathbf{H}_{\mathrm{III}}(z)\rangle = \sum_{\mathbf{k}\sigma} t_{\mathbf{k}\sigma} Y_{\mathbf{k},\sigma}|\mathbf{k}\sigma\rangle e^{ik_z z}. \quad (6)$$

As a first approximation, we assume that the perforated metallic films (regions 1 and 2 in figure 1(a)) behave as PECs. Therefore, the EM fields are different from zero only inside the holes where the EM fields can be expanded in terms of the TE and TM waveguide eigenmodes $|\alpha\rangle$ as

$$|\mathbf{E}_{(n)}(z)\rangle = \sum_{\boldsymbol{\alpha}} |\alpha\rangle [A_\alpha^{(n)} e^{iq_{z\alpha} z} + B_\alpha^{(n)} e^{-iq_{z\alpha} z}] \quad (7)$$

$$-\mathbf{u}_z \times |\mathbf{E}_{(n)}(z)\rangle = \sum_{\boldsymbol{\alpha}} |\alpha\rangle Y_\alpha^{(n)} [A_\alpha^{(n)} e^{iq_{z\alpha} z} - B_\alpha^{(n)} e^{-iq_{z\alpha} z}] \quad (8)$$

where $q_{z\alpha}$ represents the propagation constant associated with the mode α and $A_\alpha^{(n)}$ and $B_\alpha^{(n)}$ are its corresponding expansion coefficients. The admittance of the α mode is defined by $Y_\alpha = q_{z\alpha}/k_0$ for a TE mode, while for a TM mode $Y_\alpha = k_0/q_{z\alpha}$. The index n refers to the metallic layer. For indentations with simple cross sections such as rectangular or circular, the required expressions for $|\alpha\rangle$ and $q_{z\alpha}$ can be found analytically.

In the modal expansion of the EM fields inside the holes, it is convenient to relate the expansion coefficients to the quantities $E_\alpha^{(n)} = A_\alpha^{(n)} + B_\alpha^{(n)}$, $E_\alpha^{(n)'} = -\{A_\alpha^{(n)} e^{iq_z h_m} + B_\alpha^{(n)} e^{-iq_z h_m}\}$, which are the modal amplitudes of the electric field of the α mode at the input and output sides of the holes of the n metallic film, respectively. After matching appropriately the EM fields at the four interfaces, we end up with a set of four coupled linear equations for the expansion coefficients $\{E_\alpha^{(n)}, E_\alpha^{(n)'}\}$:

$$(G_{\alpha\alpha} - \Sigma_\alpha) E_\alpha^{(1)} + \sum_{\beta\neq\alpha} G_{\alpha\beta} E_\beta^{(1)} - G_\alpha^V E_\alpha^{(1)'} = I_\alpha \quad (9a)$$

$$G_\alpha^V E_\alpha^{(1)} + (Q_{\alpha\alpha} + \Sigma_\alpha) E_\alpha^{(1)'} + P_{\alpha\alpha} E_\alpha^{(2)} + \sum_{\beta\neq\alpha} [Q_{\alpha\beta} E_\beta^{(1)'} + P_{\alpha\beta} E_\beta^{(2)}] = 0 \quad (9b)$$

$$P_{\alpha\alpha} E_\alpha^{(1)'} + (Q_{\alpha\alpha} + \Sigma_\alpha) E_\alpha^{(2)} + G_\alpha^V E_\alpha^{(2)'} + \sum_{\beta\neq\alpha} [P_{\alpha\beta} E_\beta^{(1)'} + Q_{\alpha\beta} E_\beta^{(2)}] = 0 \quad (9c)$$

$$(G_{\alpha\alpha} - \Sigma_\alpha) E_\alpha^{(2)'} + \sum_{\beta\neq\alpha} G_{\alpha\beta} E_\beta^{(2)'} - G_\alpha^V E_\alpha^{(2)} = 0. \quad (9d)$$

The different terms of these equations have a simple physical interpretation. I_α measures the overlap between the incident plane wave and the α-mode of the first metal layer ($n = 1$):

$$I_\alpha = 2i Y_{\mathbf{k}_0,\sigma_0} S_{\mathrm{p},0\alpha} \quad (10)$$

where $S_{\sigma_0,0\alpha} = \langle \mathbf{k}_0\sigma_0|\alpha\rangle$. The EM coupling between the holes forming the 2D array is mediated by the term $G_{\alpha\beta}$, which can be expressed as

$$G_{\alpha\beta} = i \sum_{\sigma,\mathbf{k}} Y_{\mathbf{k},\sigma} S_{\sigma,\alpha\mathbf{k}} S_{\sigma,\mathbf{k}\beta} \quad (11)$$

where $S_{\sigma,\alpha\mathbf{k}} = \langle \mathbf{k}\sigma|\alpha\rangle$. According to Bloch's theorem, $\mathbf{k} = \mathbf{k}_0 + \mathbf{G}$, $\mathbf{G}$ being a reciprocal lattice vector. The coupling between the two sides of the holes is accounted for by $G_\alpha^V = Y_\alpha/\sin(q_{z\alpha} h_m)$ and $\Sigma_\alpha = Y_\alpha/\tan(q_{z\alpha} h_m)$ is related to the bouncing back and forth of the EM fields inside the holes. The terms

$$Q_{\alpha\beta} = \sum_{\sigma,\mathbf{k}} \frac{Y_{\mathbf{k},\sigma} S_{\sigma,\alpha\mathbf{k}} S_{\sigma,\mathbf{k}\beta}}{\tan(k_z h_d)} \quad (12)$$

$$P_{\alpha\beta} = \sum_{\sigma,\mathbf{k}} \frac{Y_{\mathbf{k},\sigma} S_{\sigma,\alpha\mathbf{k}} S_{\sigma,\mathbf{k}\beta}}{\sin(k_z h_d)} \quad (13)$$

control the coupling between the first and the second metallic films.

Once the system of equations is solved, it is straightforward to find the expansion coefficients and the EM fields in all space. From them, we can calculate the reflection and transmission coefficients. Until now, we have assumed that the material forming the perforated films is a PEC. Therefore, within this approximation, quantitative results can be obtained in the terahertz or microwave frequency regimes. At optical frequencies, the metal conductance depends on the frequency of the incident light and EM fields penetrate into the metal. The effect of this penetration can be incorporated into our formalism by using surface impedance boundary conditions (SIBCs) at the horizontal interfaces of the structure, instead of the ones associated with a perfect conductor. By using these approximated boundary conditions, the final system of equations for the expansion coefficients does not change with respect to equations (9*a*)–(9*d*) if $E^{(n)}$ and $E_\alpha^{(n)'}$ are now the modal expansion of $\mathbf{E}_\parallel - Z_s(-\mathbf{u}_z \times \mathbf{H}_\parallel)$ and $\mathbf{E}_\parallel + Z_s(-\mathbf{u}_z \times \mathbf{H}_\parallel)$ respectively. $Z_s = 1/\sqrt{\epsilon(\lambda)}$ is the surface impedance of the metal. The different terms feeding the system of equations take the following expressions:

$$I_\alpha = 2i \frac{Y_{\mathbf{k}_0,\sigma_0} S_{\mathrm{p},0\alpha}}{1 + Z_s Y_{\mathbf{k}_0,\sigma_0}} \quad (14)$$

$$G_{\alpha\beta} = i \sum_{\sigma,\mathbf{k}} \frac{Y_{\mathbf{k},\sigma} S_{\sigma,\alpha\mathbf{k}} S_{\sigma,\mathbf{k}\beta}}{1 + Z_s Y_{\mathbf{k},\sigma}} \quad (15)$$

$$G_\alpha^V = \frac{2i Y_\alpha e^{iq_{z\alpha} h_m}}{e^{2iq_{z\alpha} h_m}(1 + Z_s Y_\alpha)^2 - (1 - Z_s Y_\alpha)^2} \quad (16)$$

$$\Sigma_\alpha = i Y_\alpha \frac{e^{2iq_{z\alpha} h_m}(1 + Z_s Y_\alpha) + (1 - Z_s Y_\alpha)}{e^{2iq_{z\alpha} h_m}(1 + Z_s Y_\alpha)^2 - (1 - Z_s Y_\alpha)^2} \quad (17)$$

$$Q_{\alpha\beta} = i \sum_{\sigma,\mathbf{k}} Y_{\mathbf{k},\sigma} S_{\sigma,\alpha\mathbf{k}} S_{\sigma,\mathbf{k}\beta} \times \frac{e^{2ik_z h_d}(1 + Z_s Y_{\mathbf{k},\sigma}) + (1 - Z_s Y_{\mathbf{k},\sigma})}{e^{2ik_z h_d}(1 + Z_s Y_{\mathbf{k},\sigma})^2 - (1 - Z_s Y_{\mathbf{k},\sigma})^2} \quad (18)$$

$$P_{\alpha\beta} = \sum_{\sigma,\mathbf{k}} \frac{2i Y_{\mathbf{k},\sigma} S_{\sigma,\alpha\mathbf{k}} S_{\sigma,\mathbf{k}\beta} e^{ik_z h_d}}{e^{2ik_z h_d}(1 + Z_s Y_{\mathbf{k},\sigma})^2 - (1 - Z_s Y_{\mathbf{k},\sigma})^2}. \quad (19)$$

In our study, the dielectric function $\epsilon(\lambda)$ is taken from the Palik's handbook [20].

The great advantage of this modal expansion method is that, when dealing with subwavelength holes, a very good approximation to the transmission and reflection properties can be achieved by considering only the least decaying evanescent mode inside the holes (the TE_{01} mode for the chosen polarization of the incident plane wave). This allows

a semi-analytical treatment of equations (9) and to extend the formalism to study a large number of metallic films, as done at the end of this paper.

In order to check the validity of our formalism and their approximations, we have carried out some calculations on one the DF structures showing NRI in the near-infrared frequency regime [14]. In figure 1(b) we compare the results obtained with our modal expansion (dot–dashed line) with the ones using a more accurate theoretical framework, such as the finite-difference time domain (FDTD) method (solid and dashed lines). The solid line corresponds to the calculation for a perforated dielectric layer whereas the dashed line shows the result for a non-perforated dielectric layer. The fact that these two last curves are quite similar demonstrates that to consider a non-perforated dielectric film (as done in our modal expansion approach) is an accurate enough approximation. On the other hand, the agreement obtained between the dot–dashed and dashed lines in the spectral region of interest (gray area in figure 1(b), where the effective refractive index is negative) makes us confident regarding the reliability of our approach to underpin the physical mechanisms behind NRI in DF structures.

3. Results

Once we have shown that our theoretical framework is able to deal accurately with the transmission properties of DF systems in the near-infrared or optical ranges of the EM spectrum, we will concentrate on results obtained within the PEC approximation, in which it is easier to underpin the physical mechanisms behind the NRI phenomenon. To further simplify the discussion, we will also consider the case in which the dielectric film between the metallic slabs is air or vacuum ($\epsilon_{\rm d} = 1$).

In figure 2(a) we render the normal incidence transmission spectrum (transmission normalized to the amount of light impinging at the unit cell of the structure versus wavelength) for a single metallic layer perforated with a 2D hole array. As we are working within the PEC approximation, all lengths in our system are scalable and from now on we will use the period of the array, d, as the unit length in our structures. The geometrical parameters of the structure analyzed in figure 2(a) are $a_x = a_y = 0.33d$ and the thickness of the metal layer $h_1 = 0.15d$. This transmission spectrum is the typical one associated with the EOT phenomenon in PEC systems, namely, two transmission peaks reaching 100% transmission whose spectral locations appear close to the period of the array. As explained in detail in [4], these two transmission peaks stem from the excitation of two surface EM modes. These two resonances correspond to the symmetric and anti-symmetric combinations of the two spoof SPPs excited at the two surfaces of the metallic film.

When a dielectric gap is placed between two perforated PECs, a new resonant feature appears in the transmission spectrum (see figure 2(b)). In this case, the size of the holes is the same as in panel (a) but now the thicknesses of the two metallic films and the air gap are $h_{\rm m} = h_{\rm d} = 0.05d$. In this way, the total thickness of the structure is the same as

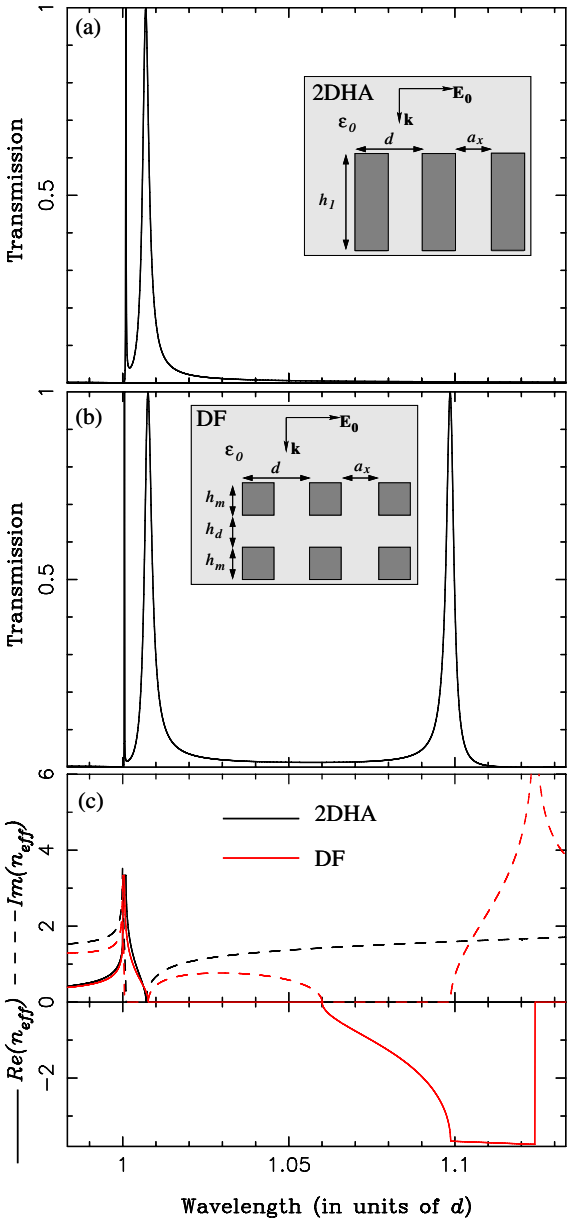

Figure 2. (a) Normalized-to-unit-cell transmittance versus wavelength for a 2D hole array (2DHA) perforated on a PEC film of thickness $h_1 = 0.15d$. The holes are square: $a_x = a_y = 0.33d$. (b) Transmittance versus wavelength for a DF structure in which the size of the holes is the same as in panel (a) but the thicknesses of the metallic films and air slab are $h_{\rm m} = h_{\rm d} = 0.05d$. (c) Effective refractive index (real and imaginary parts) associated with the two structures analyzed in panels (a) and (b).

the single perforated metallic layer studied in figure 2(a). The new transmission peak is located at a longer wavelength and we will discuss its physical origin later. What is important is the link between this new resonance and the NRI response of the DF structure, as highlighted in figure 2(c). This panel demonstrates the close correspondence between the spectral location of the long-λ transmission resonance and the region in which the effective refractive index of the structure is negative. This effective refractive index has been retrieved from the knowledge of the transmission and reflection coefficients by using the method described in [21].

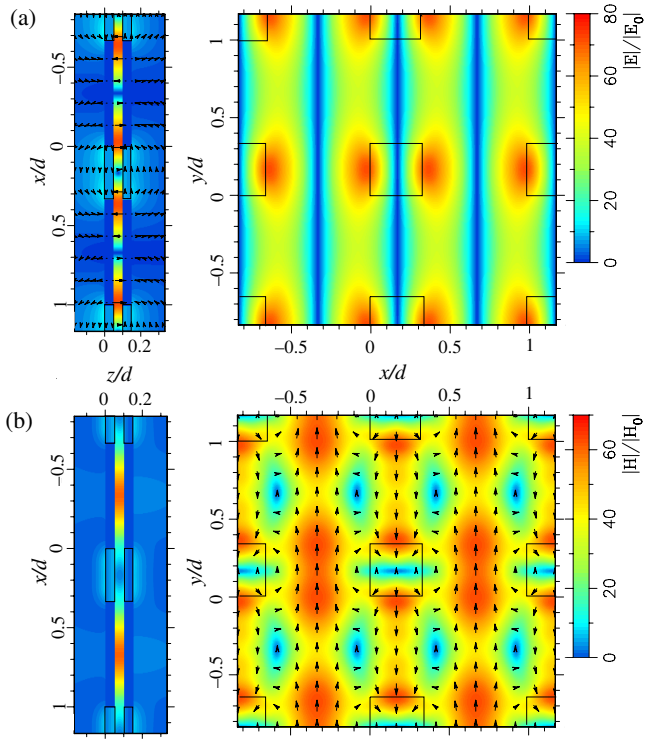

Figure 3. Electric field (a) and magnetic field (b) patterns evaluated at the resonant wavelength ($\lambda \approx 1.1d$) for the DF structure analyzed in figures 2(b). Left pictures correspond to the patterns evaluated at an xz plane that passes through the center of the holes. In the right pictures the EM fields are displayed in an xy plane placed just in the middle of the air gap.

In order to search for the physical origin of the resonance responsible for the NRI in the DF structure, it is convenient to look at their associated EM fields. This is done in figure 3, where we render the amplitudes of the electric (panel (a)) and the magnetic (panel (b)) fields calculated at the resonant wavelength ($\lambda \approx 1.1d$). The left pictures correspond to the EM field patterns evaluated at an xz plane that passes through the center of the holes, whereas in the right pictures the EM fields are calculated in an xy plane placed just in the middle of the air gap. As seen in the left panels, both the electric and magnetic fields are mainly concentrated in the air gap region. On the other hand, as shown in the right picture of figure 3(a), the electric field associated with this resonance has a strong standing wave character in the x-direction. These results suggest that the resonance responsible for the NRI response is a gap-SPP mode running at the dielectric layer placed between the two metallic films [22]. As in the structure we are analyzing the metallic films behave as PECs, we could call them *spoof* gap-SPP modes. Its origin does not stem from the finite dielectric constant of the metal as in the case of *real* gap-SPP modes but it relies on the existence of a 2D hole array drilled on the PEC films.

Now we analyze the dependence of the NRI response on the geometrical parameters of the 2D hole array, in particular of a_y. In figure 4 we study the evolution of the transmission spectrum and the corresponding effective optical parameters ($\epsilon_{\rm eff}$, $\mu_{\rm eff}$ and $n_{\rm eff}$) when a_x is fixed ($a_x = 0.33d$) and a_y is varied between $a_y = 0.42d$ and $0.75d$. The thickness of the DF structure is the same as in previous cases ($h_{\rm m} = h_{\rm d} = 0.05d$). This evolution can be understood by revisiting the concept of spoof SPP modes. As explained before, in [7], it was demonstrated that the dielectric response (in the effective medium limit in which diffraction effects are neglected) of a semi-infinite holey PEC presents a Drude-like behavior in which the plasma frequency of the electron gas is replaced by the cut-off frequency of the hole waveguide. Regarding the magnetic response, the effective magnetic permeability, $\mu_{\rm eff}$ takes a constant value. In mathematical terms, these two last sentences translate into

$$\epsilon_{\rm eff} = \frac{1}{S^2}\left(1 - \frac{\omega_{\rm p}^2}{\omega^2}\right)\mu_{\rm eff} = S^2 \qquad (20)$$

where $S = 2\sqrt{2a_x a_y}/\pi d$ and $\omega_{\rm p} = \pi c/a_y$. The magnetic permeability, $\mu_{\rm eff}$, is just a constant value. This equation implies that the cut-off wavelength, $\lambda_{\rm C} = 2a_y$, also marks the separation between positive and negative values of $\epsilon_{\rm eff}$ for a semi-infinite perforated PEC. Remarkably, this is quite close to what we observe in panel (b) of figure 4, that displays the evolution of $\epsilon_{\rm eff}$ as a_y is increased in a DF structure. The spectral location in which the real part of $\epsilon_{\rm eff}$ changes from positive to negative values (marked by vertical dashed lines) appears quite close to $\lambda_{\rm C}$. The small displacement with respect to this $\lambda_{\rm C}$ is due to the fact that in a DF structure the thicknesses of the two metallic films are finite. On the other hand, the magnetic permeability (see panel (d)) has a resonant response that, as explained above, is associated with the excitation of spoof gap-SPP modes in the air gap. Although the spectral location of the magnetic response also depends on a_y (the dispersion relation of the spoof gap-SPP mode is expected to be controlled by the geometry of the hole array), its evolution is less dramatic than the change in $\epsilon_{\rm eff}$ when a_y is increased. As expected, negative values of $n_{\rm eff}$ (see panel (c)) appear in regions in which both $\epsilon_{\rm eff}$ and $\mu_{\rm eff}$ are negative. Interestingly, when a_y is very large (for the set of geometrical parameters we are considering, $a_y = 0.75d$) there is no NRI region in the spectrum. This is due to the fact that the cut-off wavelength is longer than the spectral location of the spoof gap-SPP mode responsible for the resonant magnetic response.

The fact that DF structures display NRI behavior at near-infrared and optical frequencies is quite interesting; however, they are not truly 3D metamaterials as their thicknesses are much smaller than the operating wavelength [23]. Therefore, the question of what happens to the NRI behavior of DF-based structures when many metal–dielectric–metal stacks are added is timely and important from both the fundamental and applied points of view. In what follows, we address this issue by making use of our modal expansion technique in which the inclusion of many multilayers is straightforward. In figure 5 we plot the evolution of the transmission spectra as the number of dielectric layers, N, is increased from one (the case we have analyzed up to now) to four. The geometrical parameters of the 2D hole array we have used in these simulations are the same as the ones used in figure 2(b). As clearly seen in this

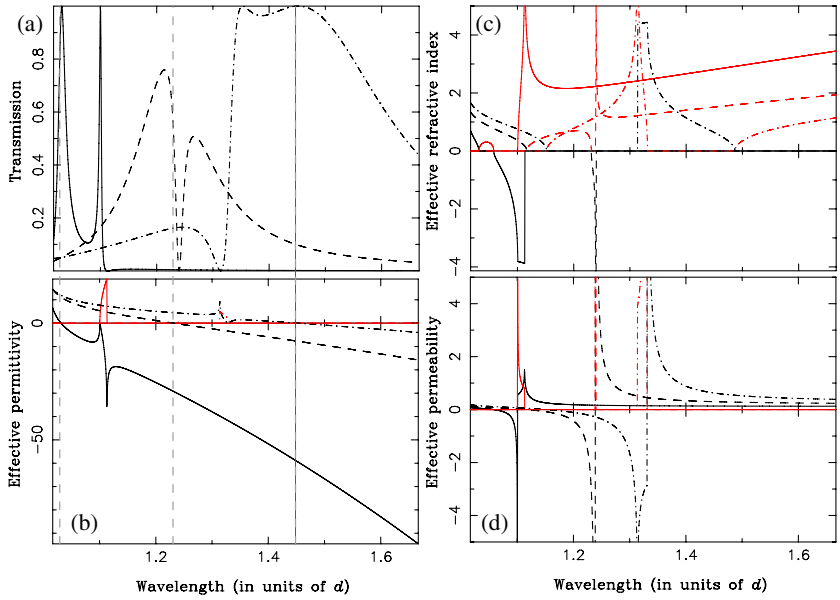

Figure 4. (a) Normal incidence transmission, (b) effective permittivity ($\epsilon_{\rm eff}$), (c) refractive index, $n_{\rm eff}$, and (d) magnetic permeability, $\mu_{\rm eff}$, for a DF structure in which $h_{\rm m} = h_{\rm d} = 0.05d$ and $a_x = 0.33d$. The different curves correspond to different values of a_y: $a_y = 0.42d$ (solid lines), $a_y = 0.58d$ (dashed lines) and $a_y = 0.75d$ (dot–dashed lines). Black curves: real parts of the effective optical parameters. Red curves: imaginary parts.

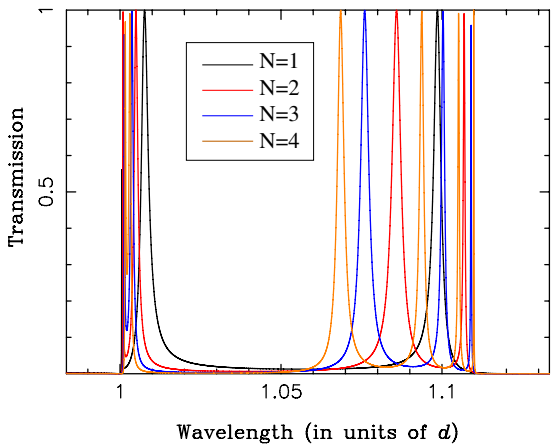

Figure 5. Transmittance versus wavelength for DF-based structures in which the number of air gaps, N, is increased from one to four. The geometrical parameters of these DF-based systems are the same as the ones used for studying a single DF structure in figure 2(b).

figure, the inclusion of more and more layers results in the appearance of additional resonant features in the transmission spectrum. The number of these new features exactly coincides with the number of dielectric layers, N. Associated with these transmission peaks, resonant behaviors of the magnetic response, $\mu_{\rm eff}$, leading to negative values are also observed. Note that the EOT peaks associated with the two surface EM modes of the entrance and exit surfaces of the structure are still present in the transmission spectrum but their linewidths are strongly reduced as N is increased.

The fact that the number of transmission peaks coincides with N suggests that the origin of the multiple transmission peaks stems from the electromagnetic coupling between the spoof gap-SPP modes running at the air gap regions. These localized modes are electromagnetically connected via the 2D hole arrays of the PEC layers. This hypothesis is nicely corroborated by figure 6, which shows the E-field amplitude patterns (evaluated at an xz plane that passes through the center of the holes) for the first four resonances appearing for the case $N = 10$. These patterns look like the different waveguide modes appearing in a Fabry–Perot cavity. They present standing wave character both in the x-direction (coming from the interference between two counter-propagating gap SPP-like modes) and in the z direction, typical of Fabry–Perot-like resonance. The first resonance (appearing for this set of parameters at $\lambda = 1.049d$) is the fundamental mode in which no nodes are present in the z-direction. As the wavelength is increased (see panels (c)–(e)), more and more nodes emerge in the pattern. These four panels highlight the collective nature of the EM modes involved in the NRI response of multilayered DF structures.

In the structure analyzed in figure 6 ($N = 10$), the thickness of the whole structure is still of the order of the wavelength. The final system we want to present in this paper is a truly DF-based 3D metamaterial. In figure 7 we render the transmission spectrum (in this case transmission versus photon energy in eV) for a DF-based structure with $N = 200$ air gaps. The geometrical parameters are the same as in previous cases and we have used $d = 600$ nm as the period of the hole array. As expected, many transmission peaks located within a very narrow energy range emerge in the spectrum. The linewidth of this NRI band (marked with label 2 in figure 7) is of the order of 50 nm. Interestingly, there is another NRI band (marked with label 1) appearing at higher frequencies. These results are corroborated by FDTD calculations on the infinite DF structure. The inset of figure 7 displays the dispersion relation (frequency versus momentum in the z-direction) of these NRI bands as calculated with the FDTD

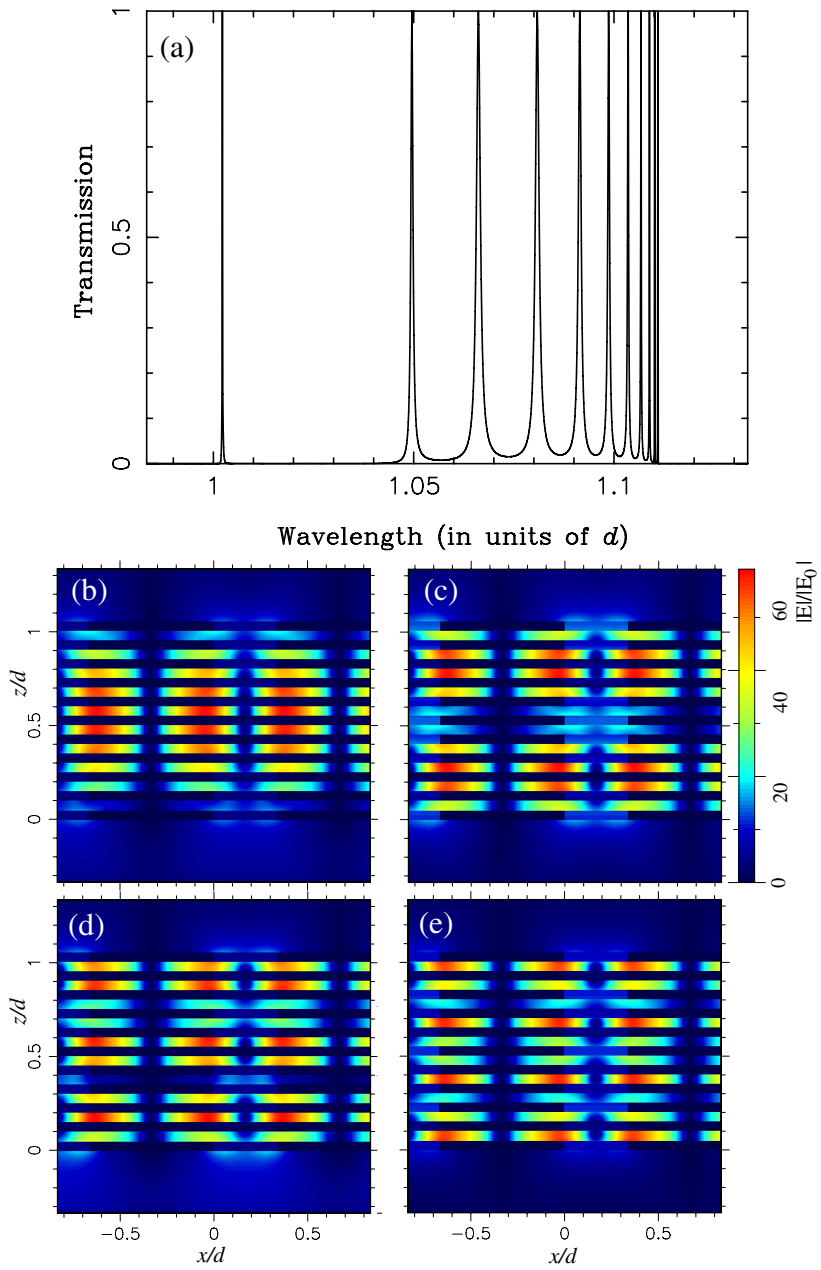

Figure 6. (a) Transmittance versus wavelength for the case $N = 10$. The geometrical parameters are the same as the ones used in previous cases. Panels (b)–(e) display the amplitude of electric field patterns for (b) $\lambda = 1.049d$ (first peak), (c) $\lambda = 1.066d$ (second peak), (d) $\lambda = 1.081d$ (third peak) and (e) $\lambda = 1.092d$ (fourth peak) evaluated in an xz plane that cuts the holes passing through their centers.

method. There is an excellent agreement between the FDTD and modal expansion results that shows again the reliability of our theoretical framework. More importantly, these results demonstrate that the NRI behavior in DF structures in PECs is maintained as the number of DF layers is increased. Note that in real metals in the optical or near-infrared regimes the presence of absorption within the metal layer would limit strongly the NRI response in multilayered DF-based structures.

4. Conclusions

We have analyzed in detail the physical mechanisms leading to the negative refractive index response observed in double-fishnet structures made of perfect electrical conductors. We have found that the electric response is mainly controlled by the cut-off frequency of the hole waveguide, which marks the separation between positive and negative values for the effective electric permittivity. On the other hand, the resonant magnetic response that yields negative values for the magnetic permeability is due to the excitation of gap-SPP-like modes propagating along the dielectric gap. We have related these two properties to two other phenomena that appear when a metallic film is perforated with a periodic array of holes: the phenomenon of extraordinary optical transmission and the emergence of spoof surface plasmon modes in perforated perfect conductors. We have also analyzed how the negative refractive index response evolves when many double-fishnet units are stacked together. Multiple magnetic resonances

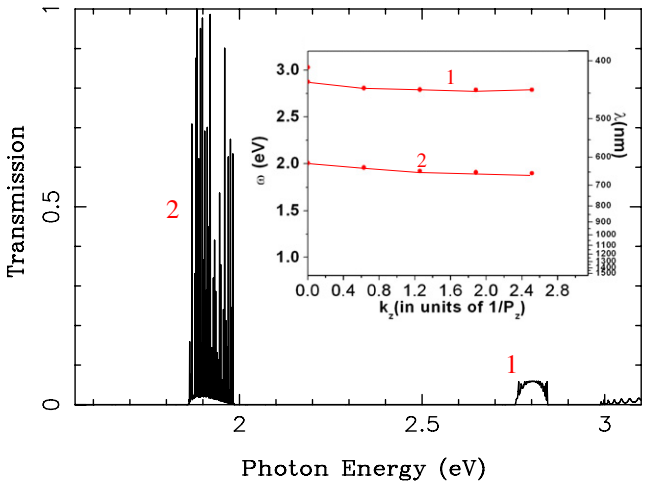

Figure 7. Transmission versus photon energy (in eV) for a multilayered DF-based structure in which the number of air gaps is $N = 200$. The 200 peaks within the energy window 1.87–1.98 eV should reach 100% transmission. The inset shows the dispersion relations (energy versus momentum in the z-direction) for the two NRI bands as calculated with the FDTD method.

emerge in these structures originated from the electromagnetic coupling between the different gap surface modes of the dielectric gaps. Finally, we have shown that in a truly 3D DF-based metamaterial the negative refractive index behavior is maintained.

References

[1] Ebbesen T W, Lezec H J, Ghaemi H F, Thio T and Wolff P A 1998 *Nature* **391** 667

[2] Genet C and Ebbesen T W 2007 *Nature* **445** 39

[3] Ghaemi H F, Thio T, Grupp D E, Ebbesen T W and Lezec H J 1998 *Phys. Rev.* B **58** 6779

[4] Martín-Moreno L, García-Vidal F J, Lezec H J, Pellerin K M, Thio T, Pendry J B and Ebbesen T W 2001 *Phys. Rev. Lett.* **86** 1114

[5] Martín-Moreno L and García-Vidal F J 2004 *Opt. Express* **12** 3619–28

[6] Beruete M, Sorolla M, Campillo I, Dolado J S, Martín-Moreno L, Bravo-Abad J and García-Vidal F J 2004 *Opt. Lett.* **29** 2500

[7] Pendry J B, Martín-Moreno L and García-Vidal F J 2004 *Science* **305** 847
García-Vidal F J, Martín-Moreno L and Pendry J B 2005 *J. Opt. A: Pure Appl. Opt.* **7** S97–101

[8] Pendry J B, Holden A J, Robbins D J and Stewart W J 1999 *IEEE Trans. Microw. Theory Tech.* **47** 2075

[9] For a recent review on negative-index metamaterials, see Shalaev V M 2007 *Nat. Photon.* **1** 41

[10] Pendry J B 2000 *Phys. Rev. Lett.* **85** 3966

[11] Zhang S, Fan W, Panoiu N C, Osgood R M and Brueck S R J 2005 *Phys. Rev. Lett.* **95** 137404

[12] Zhang S, Fan W, Malloy K J, Brueck S R J, Panoiu N C and Osgood R M 2005 *Opt. Express* **13** 4922

[13] Soukoulis C M, Linden S and Wegener M 2007 *Science* **315** 47

[14] Dolling G, Enkrich C, Wegener M, Soukoulis C M and Linden S 2006 *Opt. Lett.* **31** 1800–2

[15] Dolling G, Enkrich C, Wegener M, Soukoulis C M and Linden S 2006 *Science* **312** 892

[16] Beruete M, Sorolla M and Campillo I 2006 *Opt. Express* **14** 5445

[17] Kafesaki M, Tsiapa I, Katsarakis N, Koschny Th, Soukoulis C M and Economou E N 2007 *Phys. Rev.* B **75** 235114

[18] Bravo-Abad J, García-Vidal F J and Martín-Moreno L 2004 *Phys. Rev. Lett.* **93** 227401

[19] Mary A, Rodrigo S G, Martín Moreno L and García-Vidal F J 2007 *Phys. Rev.* B **76** 195414

[20] Palik E D (ed) 1985 *Handbook of Optical Constants of Solids* (Orlando, FL: Academic)

[21] Smith D R, Schultz S, Markos P and Soukoulis C M 2002 *Phys. Rev.* B **65** 195104

[22] Economou E N 1969 *Phys. Rev.* **182** 539

[23] Dolling G, Wegener M and Linden S 2007 *Opt Lett.* **32** 551–3